Multimodal Spectroscopic Study of Amyloid Fibril Polymorphism

Corianne C. VandenAkker,[1†] Michael Schleeger,[2$] Anne L. Bruinen,[1‡] Tanja Deckert-Gaudig,[3] Krassimir P. Velikov,[4,5] Ron M.A. Heeren,[1‡] Volker Deckert,[3,6] Mischa Bonn,[2]* Gijsje H. Koenderink[1]**

AUTHOR ADDRESSES

[1]FOM Institute AMOLF, Science Park 104, 1098 XG Amsterdam, The Netherlands.

[2]Department of Molecular Spectroscopy, Max Planck Institute for Polymer Research, Ackermannweg 10, 55128 Mainz, Germany.

[3]Leibniz Institute of Photonic Technology, Albert-Einstein-Straße 9, 07745 Jena, Germany.

[4]Soft Condensed Matter, Debye Institute for Nanomaterials Science, Department of Physics and Astronomy, Utrecht University, Princetonplein 5, 3584 CC Utrecht, The Netherlands.

[5]Unilever R&D Vlaardingen, Olivier van Noortlaan 120, 3130 AC Vlaardingen, The Netherlands.

[6]Institute for Physical Chemistry and Abbe Center of Photonics, University of Jena, Helmholtzweg 4, 07743 Jena, Germany.

[†]Current address: Department of Chemistry, Stanford University, Stanford CA 94305-5080, USA.

[$]Current address: Institute of Biochemistry and Biotechnology, Martin-Luther-Universität Halle-Wittenberg, Kurt-Mothes-Str. 3, 06120 Halle (Saale), Germany.

[‡]Current address: Maastricht MultiModal Molecular Imaging Institute, Maastricht University, Universiteitssingel 50, 6229 ER Maastricht, the Netherlands.

ABSTRACT

Amyloid fibrils are a large class of self-assembled protein aggregates that are formed from unstructured peptides and unfolded proteins. The fibrils are characterized by a universal β-sheet core stabilized by hydrogen bonds, but the molecular structure of the peptide subunits exposed on the fibril surface is variable. Here we show that multimodal spectroscopy using a range of bulk- and surface-sensitive techniques provides a powerful way to dissect variations in the molecular structure of polymorphic amyloid fibrils. As a model system, we use fibrils formed by the milk protein β-lactoglobulin, whose morphology can be tuned by varying the protein concentration during formation. We investigate the differences in the molecular structure and composition between long, straight versus short, worm-like fibrils. We show, using mass spectrometry, that the peptide composition of the two fibril types is similar. The overall molecular structure of the fibrils probed with various bulk-sensitive spectroscopic techniques shows a dominant contribution of the β-sheet core, but no difference in structure between straight and worm-like fibrils. However, when probing specifically the surface of the fibrils with nanometer resolution using tip-enhanced Raman spectroscopy (TERS), we find that both fibril types exhibit a heterogeneous surface structure with mainly unordered or α-helical structures and that the surface of long, straight fibrils contains markedly more β-sheet structure than the surface

of short, worm-like fibrils. This finding is consistent with previous surface-specific vibrational sum-frequency generation (VSFG) spectroscopic results (VandenAkker, C. C.; Engel, M. F. M.; Velikov, K. P.; Bonn, M.; Koenderink, G. H. *J. Am. Chem. Soc.* **2011,** *133*, 18030-18033). In conclusion, only advanced vibrational spectroscopic techniques sensitive to surface structure like TERS and VSFG are able to reveal the difference in structure that underlies the distinct morphology and rigidity of different amyloid fibril polymorphs that have been observed for a large range of food and disease-related proteins.

INTRODUCTION

Most, if not all, proteins and peptides are capable of self-assembling into fibrillar aggregates known as amyloids[2]. Amyloid fibrils are found in plaques in organs of patients suffering from diseases like type II diabetes mellitus and Alzheimer's disease.[3] However, Nature also makes functional use of the superior mechanical properties of amyloid fibrils, which are for instance found on the surfaces of fungi and bacteria.[4,5] Their superior mechanical properties also make amyloid fibrils interesting for synthetic biomaterials.[6-9] Amyloid fibrils are characterized by a universal cross-β structure, in which the peptide backbones are orthogonal to the fibril axis.[10,11] Hydrogen bonds stabilize the β-sheet parallel to the fibril axis and are thought to be primarily responsible for the high mechanical rigidity and strength.[12] Although the structural motif of the amyloid fibril core is known, there is mounting evidence that the overall structure is more complex and highly variable. Dependent on the constituent peptide or protein, side chains may protrude from the β-sheet core.[13,14] Moreover, amyloid samples are usually polymorphic and fibrils are often composed of two or more protofilaments, resulting in flat ribbon morphologies or twisted fibrils.[15] A well-studied example is the whey protein β-lactoglobulin[16-18] (β-lg), which readily forms amyloid fibrils upon heating at acidic pH.[19,20]

Under acidic conditions, the β-lg protein is hydrolyzed, yielding a mixture of peptides that are subsequently incorporated into amyloid fibrils.[21] We have previously shown that the morphology of β-lg amyloid fibrils can be tuned by changing the protein concentration during incubation.[1] Two different fibril types were distinguished: long, straight fibrils and short, worm-like fibrils, with a factor 40 difference in persistence length. Later nanoindentation experiments proved that the straight fibrils are indeed substantially stiffer than worm-like fibrils (private communications). These observations suggest that the two fibril types differ in secondary

structure content, since prior experimental and theoretical work showed that the Young's modulus of amyloid fibrils sensitively depends on secondary structure, increasing with increasing β-sheet content.[12,22] However, it is also possible that fibrils formed at different concentrations differ in peptide composition, since the self-assembly process involves hydrolysis to form a mixture of peptides that may have different propensities of amyloid formation.[23,24]

Here, we perform a detailed spectroscopic investigation of the differences in molecular structure of the core and the surface of the straight and worm-like fibrils formed at different β-lg concentrations, combining bulk vibrational spectroscopy techniques with surface-specific vibrational spectroscopies. We focus on the amide I mode, which reports on protein secondary structure. The molecular structure of the surface was spatially mapped with high lateral resolution using tip-enhanced Raman spectroscopy (TERS) and compared to the overall secondary structure of the fibrils analyzed using Fourier-transform infrared (FT-IR), Raman and circular dichroism (CD) spectroscopy. Our TERS study reveals that the surface of straight amyloid fibrils formed at low β-lg concentration has a higher average β-sheet content than the surface of worm-like fibrils formed at high β-lg concentration. Moreover, both fibril types exhibit a heterogeneous surface structure. However, with bulk spectroscopic techniques (Raman, FT-IR and CD spectroscopy), it is not possible to detect differences between the fibril types because these techniques mainly pick up the β-sheet signature from the fibril core. We conclude that straight and worm-like amyloid fibrils differ in their surface structure while their bulk structure and molecular composition are comparable. Given that mass spectrometry analysis reveals the peptide composition of both fibril types to be nearly identical, it is the difference in secondary structure that underlies their large difference in shape and rigidity.

MATERIALS AND METHODS

Amyloid fibril formation. β-lactoglobulin (β-lg) amyloid fibrils were prepared as described previously[1]. In brief, bovine β-lg (genetic variants A and B, Sigma Aldrich, L0130) was dissolved in HCl solution (pH=2.0). The solution was dialyzed extensively (Slide-a-lyzer, molecular weight cut-off (MWCO) 10kDa, Thermo) against an HCl solution (pH=2.0) and filtered (0.1 μm filter, Millipore) to remove aggregates. The final protein concentration was determined by UV-VIS spectrophotometry (Nanodrop, Thermo Scientific) at a wavelength of 280 nm based on an extinction coefficient of 16.8 mM^{-1} cm^{-1}.[25] Samples were heated in Eppendorf tubes at protein concentrations between 3.0 and 7.5% (w/w) in an oven at 80^{o}C for 16 hrs without stirring. After quenching in ice water, the fibrils were separated from non-aggregated material by centrifugal filtering (Centrifugal filters, MWCO 100kDa, Millipore) at 1000 g. The retentate was washed with an HCl solution (pH=2) two additional times. The filtered fibril suspension was centrifuged for 5 min at 2000 g to remove large fibril aggregates. To determine the final protein concentration, fibril suspensions were mixed with an equal volume of formic acid to solubilize the aggregated protein. The protein contents of these solutions were measured by spectrophotometry at a wavelength of 280 nm and compared to samples with known concentrations of β-lg.[26]

Atomic force microscopy (AFM). A drop of a diluted fibril suspension at a concentration of ~0.01 wt% was deposited onto freshly cleaved mica (Muscovite mica V-4, Electron Microscopy Sciences). After 5 min incubation, the sample was washed with HCl solution (pH=2.0) and dried in air. AFM images were acquired in tapping mode with a Dimension 3100 Scanning Probe Microscope (Bruker) using silicon cantilevers (TESPA, force constant 42 N/m, Bruker). Images

were flattened with a first order polynomial using Nanoscope 6.14 software to remove tilt from the image.

Mass spectrometry. Mass spectrometry experiments were performed according to the protocol of Akkermans et al.[21] Fibrils were dissolved by mixing in 0.15 M Tris-HCl buffer (pH=8.0) containing 8 M guanidine hydrochloride and 0.1 M dithiothreitol (DTT) and incubation for 1 hr. The solution was diluted in 50% (v/v) acetonitrile and 0.1% (v/v) TFA. 2 μL of the diluted sample was mixed with 18 μL of the matrix solution dimethoxy-4-hydroxycinnamic acid (CHCA) and 1 μL was dry spotted onto a 96-well target plate. MALDI-TOF spectra were obtained using a SYNAPT G1 HDMS (Waters Corporation, Milford, USA), equipped with a 200 Hz Nd:YAG laser (355 nm) and operated in positive V-reflectron mode with a 100-4000 Da mass range.

Amino acid analysis. Amino acid analysis upon hydrolysis was performed by Ansynth service B.V (the Netherlands) using high performance liquid chromatography (HPLC). Amyloid fibrils were prepared by incubation for 16 hrs, followed by filtering and washing as described above.

Fourier-Transform Infrared spectroscopy. A drop of 5 μL fibril suspension was air-dried on a diamond ATR cell (single reflection, Thermo Spectra Tech, Thermo Fisher Scientific Inc.) at room temperature. ATR/FT-IR measurements were performed on a Nicolet 730 FT-IR spectrometer (Thermo Fisher Scientific Inc.) equipped with a liquid nitrogen cooled mercury cadmium telluride (MCT) detector. The spectral resolution was set to 4 cm^{-1} and for each measurement 256 spectra were averaged. The Happ-Genzel apodization function was used for the Fourier transformation. To facilitate a direct comparison between FT-IR spectra of different samples, the FT-IR spectra were normalized to the peak value of the amide I band. Quantitative secondary structure analysis of the amyloid samples based on the FT-IR absorption spectra was

performed on the basis of the vibrational amide I band between 1600 and 1700 cm^{-1}. The fitting procedure with Gaussian-shaped line widths of the spectral components was performed as described elsewhere[27] using OriginPro 8.5.1G software.

Raman spectroscopy. Samples for Raman spectroscopy were prepared by drying a drop of 5 µL fibril suspension on a silicon wafer. To yield a thick sample film, the procedure was repeated five times. Raman spectra were measured on a Bruker RFS 100/S spectrometer (Bruker Optics, Rheinstetten, Germany) equipped with a CW laser emitting at 532 nm with an output power of 20 mJ. The laser was focused onto the sample to a spot size of about 0.5 mm using a microscope (Bruker Raman Scope Senterra). For each sample spot, 5 spectra with 60 s acquisition time were averaged. The measured Raman spectra were corrected for the fluorescence signal using the LabSpec 5 software. The amide I band of the Raman spectrum of the amyloid sample prepared at 7.5% β-lg was scaled to the same intensity as the respective band of the 3.0% sample.

Circular dichroism (CD) spectroscopy. CD data were recorded using a J-815 spectrometer (Jasco) at 20°C. Filtered amyloid fibril samples were diluted in HCl solution (pH=2.0) to protein concentrations of 0.03 wt% (~17µM) and measured in cuvettes with a path length of 0.1 cm. CD spectra were collected over a wavelength range of 190-260 nm with a step size of 1 nm. Three measurements were averaged and the α-helical and β-sheet contents were determined using Dichroweb (database 7, CDSSTR, based on 48 proteins)[28,29].

Tip-enhanced Raman spectroscopy (TERS). Fibril suspensions were diluted in HCl solution (pH=2.0) to concentrations of ~0.01%. 20 µL aliquots were deposited onto cleaned glass slides, incubated for 5 min, washed with HCl solution (pH=2.0) and dried in air. TERS measurements were performed on a setup comprised of an AFM (Nanowizard II, JPK, Berlin, Germany)

mounted on an inverted microscope (Olympus IX71, Hamburg, Germany) connected to a single stage spectrograph (SP2750A, Acton Advanced, Princeton Instruments Roper Scientific, USA) with a CCD camera (Pixis 400, Princeton Instruments Roper Scientific, USA). The incident laser with λ= 532 nm (P = 0.42 mW on sample) was focused through a 40x (N.A. 1.35) oil immersion objective on the sample. The acquisition time was 10 s for all spectra. TERS tips were prepared by evaporating a 25 nm silver layer onto commercial non-contact AFM tips (NSG10, NT-MDT, Russia).

RESULTS AND DISCUSSION

Amyloid fibril morphology

Amyloid fibrils were formed by incubation of an aqueous solution of β-lactoglobulin (β-lg) monomer at pH=2.0 and 80°C for 16 hrs at different protein concentrations, ranging between 3.0% and 7.5%. We characterized the morphology of the fibrils by depositing them on a mica surface and imaging them in the dry state by atomic force microscopy (AFM) (Figure 1a-d). At the lowest concentration (3.0% β-lg), the fibrils are straight (Figure 1a) and their lengths range from a few hundred nanometers up to 5 μm (Figure 1e). The average diameter is 2.6 nm ± 1.0 nm, quantified from the maximum height in AFM images. However, the diameter distribution is rather broad, with a main population in the range of 1–3.5 nm, and a tail with thicker fibrils having diameters of 4-6 nm.[1] These thicker fibrils are composed of two or more protofilaments and show a twisted morphology. When the protein concentration is raised to 4.5% β-lg, the fibrils have a similar morphology (Figure 1b) but the length distribution shifts to smaller lengths (Figure 1f). At still higher concentration (6.0% β-lg), the fibrils are predominantly short and do

not exhibit the straight morphology observed at low concentrations (Figure 1c). A few long fibrils are still observed, but the length distribution is dominated by short fibrils (Figure 1g). At the highest protein concentration (7.5% β-lg), the fibrils are all short and worm-like (Figure 1d) and they have a beads-on-a-string type morphology (inset Figure 1d). The fibril lengths are all below 500 nm (Figure 1h) and the average diameter is 2.9 nm ± 0.6 nm. The short, worm-like fibrils are reminiscent of previously observed fibrils formed from β-lg at high ionic strength or in water-solvent mixtures.[30,31] Worm-like amyloid fibrils have also been formed from other proteins and peptides, including disease-related proteins like α-synuclein,[32] mouse prion protein[33] and β(2)-microglobulin[34].

To quantify the decreased rigidity of fibrils formed at elevated protein concentrations, we calculated the persistence length (L_p) from the end-to-end lengths (E) and contour lengths (C) of the fibrils (Figure S1). The average value of L_p decreases dramatically with the monomer concentration during fibril formation: from 3.8 μm at 3.0% β-lg to 90 nm at 7.5% β-lg. At intermediate protein concentration, we clearly observe two different fibril populations of different persistence length when we plot E^2 vs C (Inset Figure S1b). Our results are consistent with recent AFM-based nanoindentation experiments, which showed that the rigid fibrils formed at low protein concentration have a Young's modulus in the GPa range, whereas the worm-like fibrils formed at high protein concentration have a much lower Young's modulus in the MPa range (private communications). The co-existence of straight and worm-like fibrils at intermediate protein concentrations suggests that there is a gradual shift in the populations of either fibril type with increasing protein concentration.

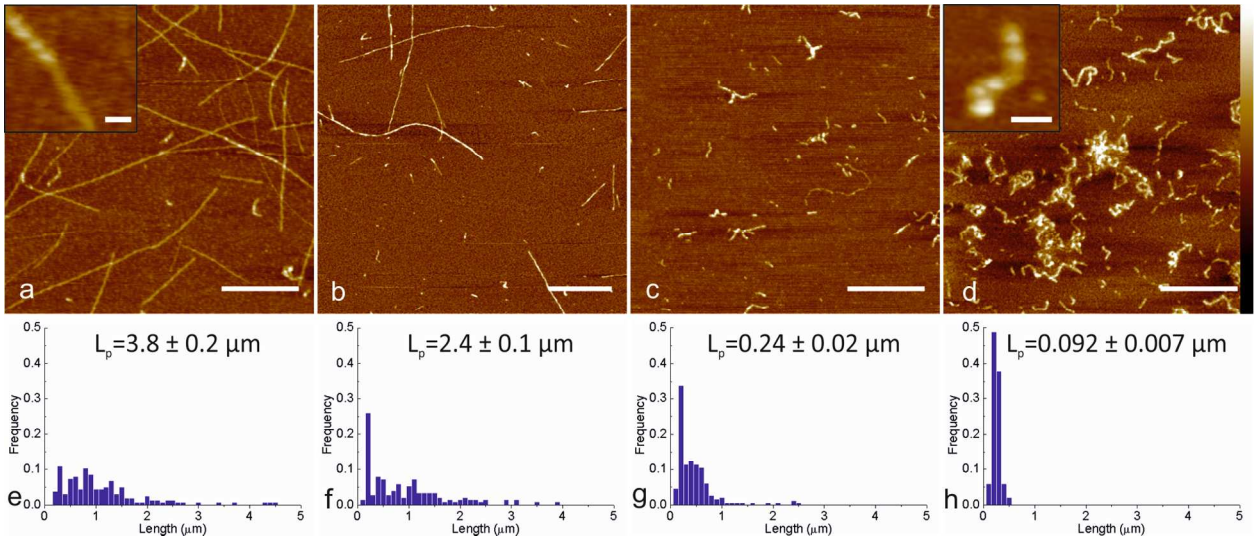

Figure 1. AFM images of β-lg amyloid fibrils on mica formed at protein concentrations of a) 3.0%; b) 4.5%; c) 6.0%; d) 7.5%. Scale bars are 500 nm, scale bars in insets are 50 nm. At 3.0% β-lg, long and straight fibrils are observed. Some fibrils are composed of two protofilaments twisted together (see inset in a). At 4.5% and 6.0% β-lg, a small fraction of long, rigid fibrils is formed, while a larger fraction contains short, flexible fibrils. At 7.5% β-lg, short, worm-like fibrils with a beaded structure (see inset in d) are formed. e-h) Length distribution of amyloid fibrils formed at β-lg concentrations of 3.0 to 7.5% ($n \geq 110$ fibrils per condition) and average persistence length L_p calculated based on the end-to-end length and the contour length measured in the AFM images. The average diameter of the fibrils was not affected by the concentration of β-lg during formation and was 2.6 ± 1.0 nm for fibrils formed at 3.0% β-lg and 2.9 ± 0.6 nm for fibrils formed at 7.5% β-lg.[1]

Molecular composition of the amyloid fibrils

Amyloid formation from β-lg at acidic pH and high temperature is known to involve hydrolysis to form a mixture of peptides. Previous mass spectrometry studies suggested that only a subset of these peptides ends up in fibrils.[21] The large difference in morphology and material properties of

the fibrils formed at different protein concentrations indicates that the composition and/or the secondary structure of the constituent peptides must be different. To test whether there is a difference in the peptide composition of the two fibril types, we compared mass spectrometry measurements on the rigid fibrils formed at 3.0% and the worm-like fibrils formed at 7.5%. After incubation of β-lg monomer for 16 hrs, the non-aggregated material was removed by filtration with 100 kDa cut-off filters. The fibrils were dissociated in guanidine chloride buffer and peptide fragments were analyzed with MALDI-TOF spectrometry according to previously published methods[21]. Incubation at pH=2 and 80° C is expected to cause cleavage of the peptide bonds between aspartic acid residues and adjacent amino acid residue.[21,35,36] The amino acid sequence of β-lg with the positions of aspartic acid (D) highlighted is depicted in Figure 2a and predicted peptide fragments are listed in Table S1. The peaks observed in the mass spectra (Figure S2) were compared to this list of candidate peptides.

We observed a high overlap of peptide fragments in straight and worm-like fibrils (Figure 2b and c). Although some minor differences in composition are observed, the entire sequence of β-lg is present in the spectra of both. This observation is in disagreement with previous results for fibrils formed at low β-lg concentrations, where only a small number of peptide fragments was observed in the fibrils.[21] The difference may be due to the slightly different protocols for fibril formation, or to a higher sensitivity towards small peptide fractions of the mass spectrometry measurements reported here. To cross-check the mass spectrometry data, we also analyzed the full amino acid composition of the filtered fibrils. This analysis revealed that the amino acid composition of both fibril types is indeed almost identical to that of the monomer (Figure 2d). This observation supports the conclusions of mass spectrometry that, although the monomer is

hydrolyzed to short peptides, all peptides end up in the fibrils. Taken together, these results show that the final peptide composition is indistinguishable for straight and worm-like fibrils.

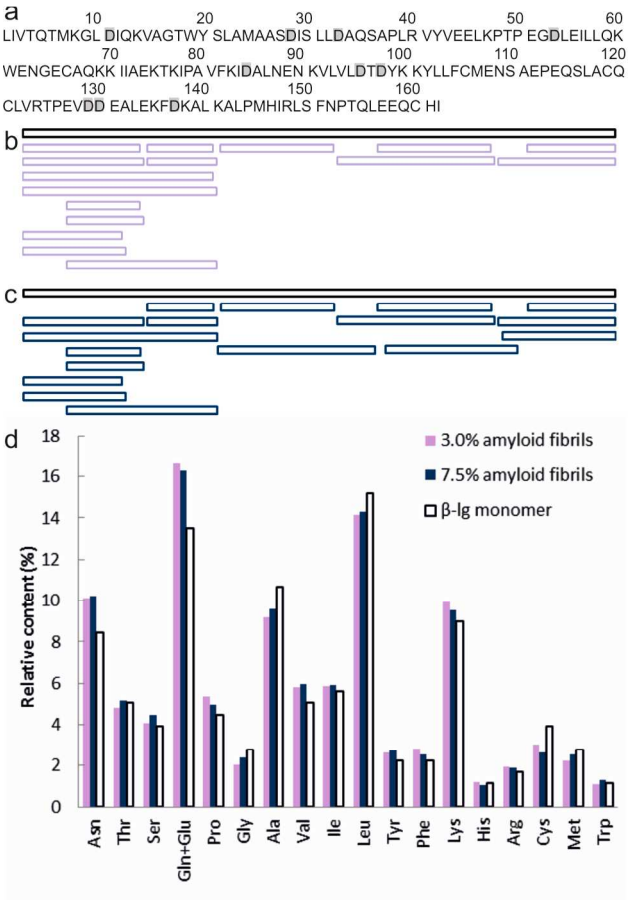

Figure 2. a) Amino acid sequence of β-lg monomer variant B. A mixture of β-lg variants A and B was used. Variant A and B differ at two sites (see Table S1). Cleavage positions are at the aspartic acid residues (D) that are highlighted. b and c) Schematic overview of peptides derived from β-lg detected in amyloid fibrils formed at protein concentrations of b) 3.0% or c) 7.5%. In black, the intact β-lg monomer (162 residues) is depicted. d) Relative amino acid content of amyloid fibrils formed at 3.0% (purple) or 7.5% (blue) determined by HPLC. White bars are the expected values based on the amino acid sequence of full-length β-lg variant B.

Bulk molecular structure of the amyloid fibrils

Given that the molecular composition of the straight and worm-like fibrils is identical, we conclude that the difference in fibril morphology and associated Young's modulus must arise from a difference in secondary structure. To test this hypothesis, we determined the molecular structure of the fibrils with four complementary spectroscopy methods: attenuated total reflection Fourier-transform infrared (ATR/FT-IR), Raman, coherent anti-Stokes Raman (CARS), and circular dichroism (CD) spectroscopy. Since all four techniques are ensemble measurements over a large number of amyloid fibrils, we chose fibril samples formed at 3.0% and 7.5% β-lg, where the populations of respectively straight fibrils and worm-like fibrils are most homogeneous.

Strikingly, the ATR/FT-IR spectra of the two fibril types are near-identical (Figure 3a). The spectral positions of the peak maxima in the amide I region around 1630 cm^{-1} indicate a high β-sheet content, as expected for amyloid samples; the main contribution of the amide I band is assigned to the low frequency band of the β-sheet structure. A quantitative secondary structure analysis[27] yielded 75% β-sheets and turns as well as 15-20% unordered or α-helical secondary structures for both fibril types (see also Figure S3).

Raman spectroscopy reports on the amide I band as well, but with a different sensitivity to the underlying vibrational normal modes. We observe that the ~1670 cm^{-1} high frequency band of the anti-parallel β-sheet structure is more pronounced in the Raman spectra of both fibril types (Figure 3b and Figure S4), compared to the ATR/FT-IR spectra, where this resonance shows up as a weak shoulder on the main ~1630 cm^{-1} band. Consistent with the FT-IR spectra, the Raman spectra show a high similarity between the amide I bands and thus secondary structure for both fibril samples. CARS measurements gave similar results for both fibril types as Raman spectroscopy (data not shown).

Finally, we determined the secondary structure of the two fibril types with CD and found 45% β-strands and -turns, 45% unordered structure and less than 10% α-helices for both samples (Figure 3c and Table S2). Again, we find no significant differences between worm-like and straight fibrils. The quantitative discrepancy between CD and the vibrational spectroscopy techniques can be explained by the weaker sensitivity of CD to β-sheets and/or the weaker sensitivity of vibrational spectroscopy to unordered structures.

Apparently, neither FT-IR, nor Raman, nor CD can detect any significant difference between the two fibril types. This is surprising, given the large difference in morphology and Young's modulus of the fibrils. Moreover, the spectroscopic equivalence of the two types of fibrils is in striking contrast with our earlier vibrational sum-frequency generation (VSFG) spectroscopy measurements of the same fibrils deposited on a mica surface, from which it was concluded that the straight fibrils are characterized by a close to 100% β-sheet content, whereas for short, worm-like fibrils the β-sheet content was only 32%, while 68% was assigned to α-helical or unordered structures.[1] Note, however that VSFG is a surface-specific technique,[37,38] while FT-IR, Raman, and CD spectroscopy are all bulk-sensitive.

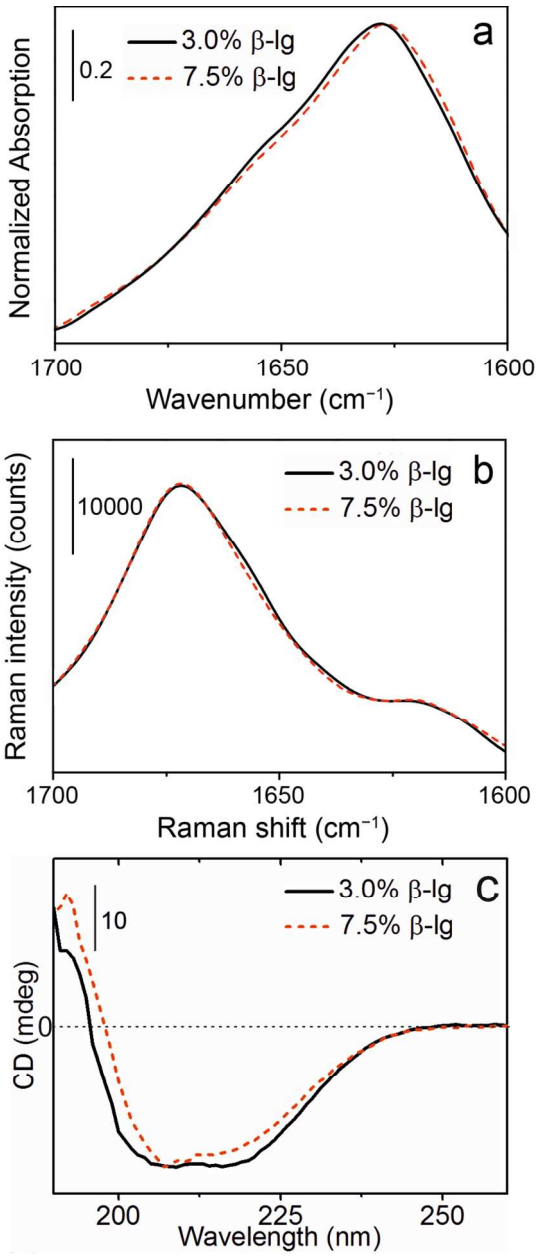

Figure 3. a) ATR/FT-IR spectra b) Raman spectra and c) CD spectra for two morphologically different types of amyloid fibrils formed at 3.0% (black) or 7.5% (red dotted) β-lg. For second derivatives and tables with fit parameters, see Table S2 and Figures S3 and S4.

Surface molecular structure of the amyloid fibrils investigated using TERS

To measure specifically the structure of the fibrils at the surface, we employed tip-enhanced Raman spectroscopy (TERS). TERS provides spectroscopic information with nanoscale spatial resolution by scanning samples with an AFM or STM tip terminated with a 10-20 nm Ag or Au particle and coupled to a Raman spectrometer.[39-44] Because of the high local field enhancement of the Raman signal, it is possible to obtain Raman spectra from the material in the immediate proximity of the metalized tip, resulting in a lateral spatial resolution in the nm scale.[45-48] Recent TERS measurements on insulin amyloid fibrils[49,50] and hIAPP amyloid fibrils[51] have demonstrated that this technique is indeed highly sensitive to the surface structure of the fibrils. Thus, TERS is an ideal technique to bridge the gap between the bulk spectroscopies described above, and the inherently surface-specific VSFG spectroscopy we reported previously. For TERS spectroscopy on β-lg amyloid fibrils, suspensions formed at β-lg concentrations of either 3.0% or 7.5% were diluted, incubated on glass slides, washed, dried and imaged (Figure 4a and b).

Figure 4a shows an AFM image of part of a rigid, straight fibril formed at 3.0% β-lg obtained with a TERS tip. The black line indicates the region along which 20 TERS spectra were obtained in spatial steps of 1 nm (Figure 4c). The secondary structure was analyzed based on the amide I region (1630-1680 cm^{-1}) of the spectra. Peaks between 1630 and 1655 cm^{-1} were assigned to unordered or α-helical structure and peaks between 1660 and 1680 cm^{-1} to β-sheets.[49,50,52,53] In some spectra, a broad peak covering both regions, or two separated peaks were observed; these spectra were assigned to a third category referred to as 'mixed' structures. The amide II band (1520-1570 cm^{-1}) and the amide III band (1230-1270 cm^{-1}) are usually weak in TERS spectra or overlap with the vibrational bands of other functional groups[49,50,52.53] and were therefore not used

for the analysis of the protein secondary structure. For comparison, a reference TERS spectra on glass was obtained (Figure S5).

The fibril shown in Fig. 4c has a remarkably heterogeneous surface structure, with some regions dominated by unordered or α-helical structure whereas other regions show β-sheet or mixed structures. For comparison, an AFM image and a grid of 10 x 5 TERS measurements on a worm-like fibril formed at 7.5% β-lg are shown (Figure 4b), again in steps of 1 nm. For clarity only the first 20 spectra are depicted in Figure 4d. The surface of this worm-like fibril is dominated by unordered/α-helical structure, but also contains small regions of mixed structures.

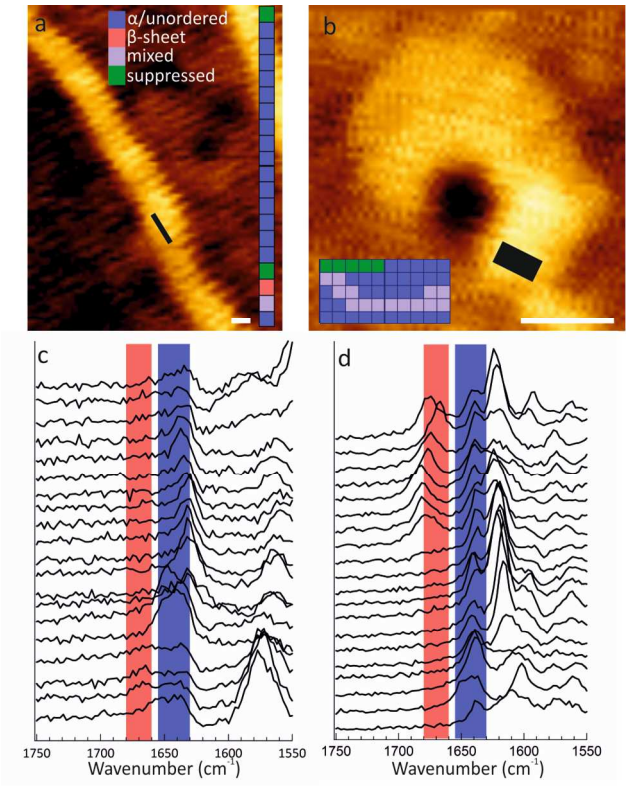

Figure 4. AFM images and corresponding TERS spectra obtained by sampling grids with 1-nm sized pixels of amyloid fibrils formed at a) 3.0% β-lg and b) 7.5% β-lg. AFM images were

obtained with an AFM tip terminated with a silver particle. Scale bars are 50 nm. c and d) Amide I region of the spectra corresponding to the regions indicated by black lines in a and b. Red band: β-sheet. Blue band: unordered/α-helical structure. For clarity, only the first 20 spectra are shown in (d), corresponding to the two bottom rows in the map in (b).

In order to compare the TERS data with ensemble measurements of the molecular structure obtained by bulk IR and Raman spectroscopy, all TERS spectra with active amide I bands were analyzed and pooled. This analysis represents an average of 10 datasets for amyloids formed at 3.0% β-lg on 4 different straight fibrils, and 8 datasets on 6 worm-like fibrils formed at 7.5% β-lg. In total more than 350 spectra per condition were collected. For straight fibrils, 112 out of 350 spectra (32%) showed suppressed amide I bands. For worm-like fibrils, the number of suppressed amide I bands was 155 out of 382 spectra (32%). This phenomenon has been observed previously in TERS studies of insulin amyloid fibrils[49,50] and hIAPP amyloid fibrils[51] and is also common in SERS experiments[54,55].

The datasets with active amide I bands (238 and 227 spectra for straight and worm-like fibrils, respectively) were analyzed for unordered/α-helical, β-sheet and mixed structures. For 66% of the spectra of the straight fibrils and 74% of worm-like fibrils, only unordered or α-helical structures were observed (Figure 5a and Table S3). For straight fibrils, 10% of the spectra were classified as β-sheet and 24% as mixed structures. For worm-like fibrils these percentages were much lower: only 5% β-sheet and 21% mixed structures.

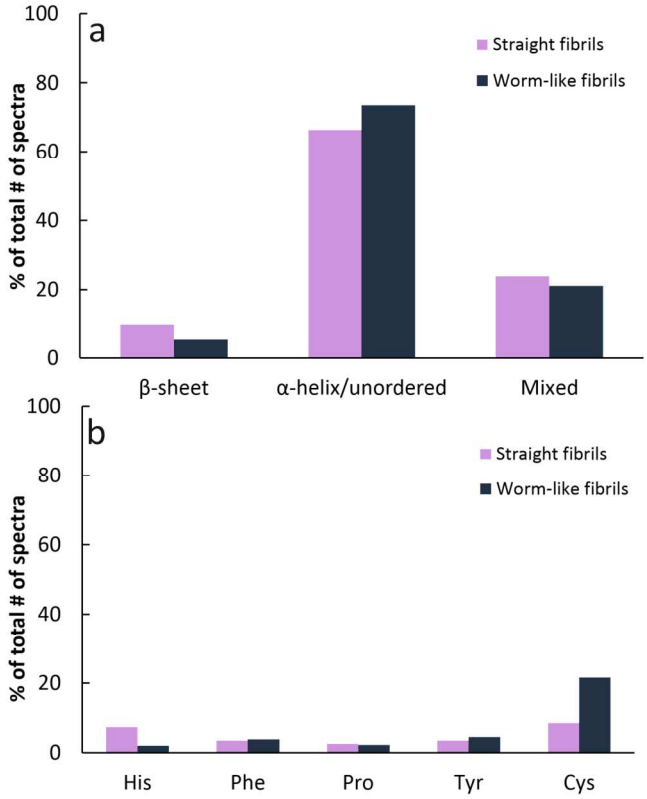

Figure 5. a) Ensemble analysis of the molecular structure observed with TERS for amyloid fibrils formed at 3.0% β-lg (purple) or 7.5% β-lg (blue). b) Ensemble analysis of the amino acid residues identified using TERS for amyloid fibrils formed at 3.0% β-lg (purple) or 7.5% β-lg (blue).

TERS cannot only be used to analyze the secondary structure of protein aggregates, but it is also possible to identify specific amino acid residues through their unique vibrational bands, and determine their position at the fibril surface.[49,50] We analyzed all spectra for peaks related to histidine (His), phenylalanine (Phe), proline (Pro), tyrosine (Tyr) and cysteine (Cys) (Table S4). Phe and Tyr were observed in 3 to 5% of all spectra for both fibril types (Figure 5b and Table S3). Pro was observed in only 2 to 3% of the spectra, although 8 of the 162 (5%) amino acid residues in β-lg monomer is Pro. This discrepancy suggests that Pro may reside preferably in the

core and not on the surface of the fibrils. For straight fibrils, His was observed much more frequently (7%) than for worm-like fibrils (2%). In both cases, this frequency is higher than expected from the amino acid sequence of β-lg, which features 2 His residues out of a total of 162 amino acids (1.2%). Cys was observed in 9% of the spectra for straight fibrils, and in 22% of the spectra for worm-like fibrils. These percentages are much higher than the expected value based on the number of Cys residues in β-lg monomer: 5 out of 162 (3.1%). Apparently Cys has a preference for the unordered or α-helical structure at the surface of the fibrils and not for the β-sheet core. This is in agreement with our TERS measurements on hIAPP amyloid fibrils[51], for which we observed Cys in 15 to 25% of all spectra, while, from simple statistics, the expected percentage was 5%.

Comparison between different spectroscopic techniques

While it is tempting to quantitatively compare the percentages of α-helical, disordered or β-sheet structure obtained using the different spectroscopies, this is complicated by the fact that all of the spectroscopies have different selection rules and sensitivities towards specific structures. Qualitatively, however, it is apparent that the bulk spectroscopies are unable to distinguish between straight and worm-like β-lg fibrils, while nonlinear and surface spectroscopies (vibrational sum frequency generation (VSFG) spectroscopy and TERS) show clear and significant differences. Specifically, it is instructive to compare the two-fold increase of the β-sheet content in straight fibrils compared to the worm-like fibrils we observe by TERS to the three-fold ratio increase we observed earlier by VSFG spectroscopy.[1] Consistent with prior TERS measurements on insulin and hIAPP fibrils,[49-51] we observe that TERS primarily probes the surface of the fibrils and to a lesser extent the β-sheet cores that are mainly measured with bulk spectroscopy. The surface is more disordered for the worm-like fibrils than for the straight

fibrils, likely because the worm-like fibrils, with their beads-on-a-string morphology, exhibit relatively short regions of hydrogen-bonded β-sheets along the long axis. Both TERS and VSFG are expected to be sensitive to interruptions of the β-sheet structure along the fiber axes. In contrast, the straight fibrils with their uniformly high rigidity along the fibril axis probably exhibit a more regular β-sheet core that is partly exposed at the surface.

These TERS data, based on more than 200 spectra for each fibril type, confirm the differences in molecular structure between straight and worm-like fibrils that we observed previously with VSFG measurements[1] (Figure S6). By VSFG we measured a nearly 100% β-sheet fraction for straight fibrils, while for worm-like fibrils the β-sheet content was much lower (32%), with a considerable contribution of α-helical or unordered structures (68%). Although TERS also reports a lower β-sheet content for worm-like fibrils than for straight fibrils, the distinction between the two fibril types is clearly more subtle in TERS compared to VSFG measurements. A possible reason is that the surface specificity of TERS is mainly based on the restriction of the field enhancement effect to the immediate vicinity of the metalized AFM tip.[39-42] In contrast, VSFG is a second order nonlinear optical technique.[37] In order for a VSFG signal to be generated, the inversion symmetry of the medium emitting the second order response has to be broken. For bulk isotropic media, this will only be the case at the interface. One may further speculate that differences in the secondary structure content determined by TERS and VSFG can be at least partly attributed to the fact that VSFG reports exclusively on the secondary structures which have a preferential alignment towards the surface normal, i.e., exclusively those for which inversion symmetry is broken.[37] In contrast, TERS reports on the resonances from the whole surface region.

In an effort to fathom the origin of VSFG signals from β-lg amyloid samples, we performed second harmonic generation (SHG) microscopy experiments. Note that the process of SHG is a special case of VSFG, and the same selection rules apply. We measured on dry amyloid films on glass, taking care to suppress any signal contribution from the bottom or top surface of the samples by making sure not to focus the fundamental beam at either of these surfaces. A clear SHG response was measured for straight fibrils, whereas the worm-like fibril samples showed an SHG response only slightly above the noise level (Figure S7). The appearance of a bulk SHG signal indicates a structural organization of the straight fibrils, for which inversion symmetry is apparently at least partially lifted. Remarkably, the difference in the signal intensities between the two samples observed for SHG was much less apparent for VSFG; for VSFG the signal strengths associated with the predominantly α-helical or unordered worm-like fibrils and the β-sheet straight fibrils was very comparable. This indicates a (weak) electronic resonance at the SHG wavelength (400nm) present in the straight fibrils, but not in the worm-like fibrils, which can tentatively be attributed to the more delocalized electron system of the better stacked β-sheet structure of the straight fibrils.

CONCLUSIONS

We investigated the structural differences between straight and worm-like amyloid fibrils made of the whey protein β-lg by AFM and a combination of surface and bulk vibrational spectroscopy techniques. AFM imaging revealed that the morphology of β-lg amyloid fibrils sensitively depends on the protein concentration during formation. At low concentration, the fibrils are long and straight, whereas at high concentration the fibrils are short and worm-like with a 40-fold lower persistence length. We hypothesized that this morphological difference could be caused by either a difference in peptide composition or in molecular structure. Mass spectrometry showed

that both fibril types are formed from peptide fragments, and the composition was near-identical in the two cases. The overall molecular structure as probed with FT-IR, Raman and CD spectroscopy was also indistinguishable for the two fibril types, with a high β-sheet content in both cases. However, surface-sensitive measurements by TERS revealed a marked difference in the surface structure of the two fibril types, corroborating previous VSFG measurements.[1] The surface of both fibril types is heterogeneous and mainly contains unordered or α-helical structures. However, the straight fibrils have a two-fold higher β-sheet content at the surface than the worm-like fibrils In conclusion, straight and worm-like fibrils have a different molecular structure, but it is only possible to probe this difference using surface-specific second-order nonlinear optical spectroscopy or surface-sensitive spectroscopic techniques, such as TERS. The difference in molecular structure is responsible for the large difference in rigidity of straight and worm-like amyloid polymorphs, which have been observed for a wide range of peptides and proteins relevant to diseases as well as applications.

ASSOCIATED CONTENT

Supporting Information. Supporting figures and tables are included in the Supporting Information. This material is available free of charge via the Internet at http://pubs.acs.org.

AUTHOR INFORMATION

Corresponding Authors

*Gijsje H. Koenderink: E-mail: gkoenderink@amolf.nl. Phone: +31-20-7547100. Fax: +31-20-7547290.

*Mischa Bonn: E-mail: bonn@mpip-mainz.mpg.de. Phone: +49 6131 379-161. Fax: +49 6131 379-360.

*Volker Deckert: E-mail: volker.deckert@uni-jena.de. Phone: +49 3641/9-48347. Fax: +49-3641/9-48302.

Author Contributions

The manuscript was written through contributions of all authors. All authors have given approval to the final version of the manuscript.

ACKNOWLEDGMENTS

We thank D. Schneider (Johannes Gutenberg Universitat, Mainz, Germany) for the kind possibility to make use of his CD spectrometer. We thank A. Kiss and S. Ellis (FOM Institute AMOLF, The Netherlands) for help with mass spectrometry experiments and Jang Hyuk Lee (MPI-P, Germany) for assistance with CARS and SHG experiments.

This work is part of the Industrial Partnership Programme (IPP) Bio(-Related) Materials (BRM) of the Stichting voor Fundamenteel Onderzoek der Materie (FOM), which is financially supported by the Nederlandse Organisatie voor Wetenschappelijk Onderzoek (NWO). The IPP BRM is co-financed by the Top Institute Food and Nutrition and the Dutch Polymer Institute. This work is also supported by NanoNextNL, a micro and nanotechnology consortium of the Government of the Netherlands and 130 partners.

REFERENCES

1. VandenAkker, C. C.; Engel, M. F. M.; Velikov, K. P.; Bonn, M.; Koenderink, G. H. Morphology and Persistence Length of Amyloid Fibrils Are Correlated to Peptide Molecular Structure. *J. Am. Chem. Soc.* **2011,** *133*, 18030-18033.
2. Knowles, T. P. J.; Vendruscolo, M.; Dobson, C. M. The Amyloid State and its Association with Protein Misfolding Diseases. *Nat. Rev. Mol. Cell Bio.* **2014,** *15*, 384-396.
3. Stefani, M.; Dobson, C. M. Protein Aggregation and Aggregate Toxicity: New Insights into Protein Folding, Misfolding Diseases and Biological Evolution. *J. Mol. Med-Jmm* **2003,** *81*, 678-699.
4. Gebbink, M.; Claessen, D.; Bouma, B.; Dijkhuizen, L.; Wosten, H. A. B. Amyloids - A Functional Coat for Microorganisms. *Nat. Rev. Microbiol.* **2005,** *3*, 333-341.
5. Otzen, D.; Nielsen, P. H. We Find Them Here, We Find Them There: Functional Bacterial Amyloid. *Cell. Mol. Life Sci.* **2008,** *65*, 910-927.
6. Cherny, I.; Gazit, E. Amyloids: Not Only Pathological Agents but Also Ordered Nanomaterials. *Angew. Chem. Int. Edit.* **2008,** *47*, 4062-4069.
7. Jones, O. G.; Mezzenga, R. Inhibiting, Promoting, and Preserving Stability of Functional Protein Fibrils. *Soft Matter* **2012,** *8*, 876-895.
8. Knowles, T. P.; Buehler, M. J. Nanomechanics of Functional and Pathological Amyloid Materials. *Nat. Nanotech.* **2011,** *6*, 469-479.
9. Li, C. X.; Born, A. K.; Schweizer, T.; Zenobi-Wong, M.; Cerruti, M.; Mezzenga, R. Amyloid-Hydroxyapatite Bone Biomimetic Composites. *Adv. Mater.* **2014,** *26*, 3207-3212.
10. Krebs, M. R. H.; Domike, K. R.; Cannon, D.; Donald, A. M. Common Motifs in Protein Self-Assembly. *Faraday Discuss.* **2008,** *139*, 265-274.
11. Tycko, R. Progress Towards a Molecular-Level Structural Understanding of Amyloid Fibrils. *Curr. Opin. Struc. Biol.* **2004,** *14*, 96-103.
12. Knowles, T. P.; Fitzpatrick, A. W.; Meehan, S.; Mott, H. R.; Vendruscolo, M.; Dobson, C. M.; Welland, M. E. Role of Intermolecular Forces in Defining Material Properties of Protein Nanofibrils. *Science* **2007,** *318*, 1900-1903.
13. Nelson, R.; Sawaya, M. R.; Balbirnie, M.; Madsen, A. O.; Riekel, C.; Grothe, R.; Eisenberg, D. Structure of the Cross-Beta Spine of Amyloid-Like Fibrils. *Nature* **2005,** *435*, 773-778.
14. van Gestel, J.; de Leeuw, S. W. The Formation of Fibrils by Intertwining of Filaments: Model and Application to Amyloid A Beta Protein. *Biophys. J.* **2007,** *92*, 1157-1163.
15. MacPhee, C. E.; Dobson, C. M. Formation of Mixed Fibrils Demonstrates the Generic Nature and Potential Utility of Amyloid Nanostructures. *J. Am. Chem. Soc.* **2000,** *122*, 12707-12713.
16. Hamada, D.; Tanaka, T.; Tartaglia, G. G.; Pawar, A.; Vendruscolo, M.; Kawamura, M.; Tamura, A.; Tanaka, N.; Dobson, C. M. Competition between Folding, Native-State Dimerisation and Amyloid Aggregation in Beta-Lactoglobulin. *J. Mol. Biol.* **2009,** *386*, 878-890.
17. Hamley, I. W. Peptide Fibrillization. *Angew. Chem. Int. Edit.* **2007,** *46*, 8128-8147.

18. Adamcik, J.; Jung, J. M.; Flakowski, J.; De Los Rios, P.; Dietler, G.; Mezzenga, R. Understanding Amyloid Aggregation by Statistical Analysis of Atomic Force Microscopy Images. *Nat. Nanotechnol.* **2010,** *5*, 423-428.
19. Bromley, E. H. C.; Krebs, M. R. H.; Donald, A. M. Aggregation Across the Length-Scales in Beta-Lactoglobulin. *Faraday Discuss.* **2005,** *128*, 13-27.
20. Gosal, W. S.; Clark, A. H.; Pudney, P. D. A.; Ross-Murphy, S. B. Novel Amyloid Fibrillar Networks Derived from a Globular Protein: β-Lactoglobulin. *Langmuir* **2002,** *18*, 7174-7181.
21. Akkermans, C.; Venema, P.; van der Goot, A. J.; Gruppen, H.; Bakx, E. J.; Boom, R. M.; van der Linden, E. Peptides Are Building Blocks of Heat-Induced Fibrillar Protein Aggregates of Beta-Lactoglobulin Formed at pH 2. *Biomacromolecules* **2008,** *9*, 1474-1479.
22. Litvinov, R. I.; Faizullin, D. A.; Zuev, Y. F.; Weisel, J. W. The Alpha-Helix to Beta-Sheet Transition in Stretched and Compressed Hydrated Fibrin Clots. *Biophys. J.* **2012,** *103*, 1020-1027.
23. Bolder, S. G.; Vasbinder, A. J.; Sagis, L. M. C.; van der Linden, E. Heat-Induced Whey Protein Isolate Fibrils: Conversion, Hydrolysis, and Disulphide Bond Formation. *Int. Dairy J.* **2007,** *17*, 846-853.
24. Kroes-Nijboer, A.; Venema, P.; Bouman, J.; van der Linden, E. Influence of Protein Hydrolysis on the Growth Kinetics of β-lg Fibrils. *Langmuir* **2011,** *27*, 5753-5761.
25. Veerman, C.; Baptist, H.; Sagis, L. M. C.; Van der Linden, E. A New Multistep Ca2+-Induced Cold Gelation Process for Beta-Lactoglobulin. *J. Agr. Food Chem.* **2003,** *51*, 3880-3885.
26. Klunk, W. E.; Jacob, R. F.; Mason, R. P. Quantifying Amyloid [beta]-Peptide (A[beta]) Aggregation Using the Congo Red-A[beta] (CR-A[beta]) Spectrophotometric Assay. *Anal. Biochem.* **1999,** *266*, 66-76.
27. Arrondo, J. L. R.; Muga, A.; Castresana, J.; Goni, F. M. Quantitative studies of the Structure of Proteins in Solution by Fourier-Transform Intrared-Spectroscopy. *Prog. Biophys. Mol. Bio.* **1993,** *59*, 23-56.
28. Whitmore, L.; Wallace, B. A. Protein Secondary Structure Analyses from Circular Dichroism Spectroscopy: Methods and Reference Databases. *Biopolymers* **2008,** *89*, 392-400;
29. Whitmore, L.; Wallace, B. A. DICHROWEB, an Online Server for Protein Secondary Structure Analyses from Circular Dichroism Spectroscopic Data. *Nucleic Acids Res.* **2004,** *32*, W668-73.
30. Gosal, W. S.; Clark, A. H.; Ross-Murphy, S. B. Fibrillar Beta-Lactoglobulin Gels: Part 1. Fibril Formation and Structure. *Biomacromolecules* **2004,** *5*, 2408-2419.
31. Arnaudov, L. N.; de Vries, R. Strong Impact of Ionic Strength on the Kinetics of Fibrilar Aggregation of Bovine Beta-Lactoglobulin. *Biomacromolecules* **2006,** *7*, 3490-3498.
32. Giehm, L.; Oliveira, C. L. P.; Christiansen, G.; Pedersen, J. S.; Otzen, D. E. SDS-Induced Fibrillation of alpha-Synuclein: An Alternative Fibrillation Pathway. *J. Mol. Biol.* **2010,** *401*, 115-133.
33. Singh, J.; Sabareesan, A. T.; Mathew, M. K.; Udgaonkar, J. B. Development of the Structural Core and of Conformational Heterogeneity during the Conversion of Oligomers of the Mouse Prion Protein to Worm-like Amyloid Fibrils. *J. Mol. Biol.* **2012,** *423*, 217-231.

34. Debelouchina, G. T.; Platt, G. W.; Bayro, M. J.; Radford, S. E.; Griffin, R. G. Magic Angle Spinning NMR Analysis of beta(2)-Microglobulin Amyloid Fibrils in Two Distinct Morphologies. *J. Am. Chem. Soc.* **2010,** *132*, 10414-10423.
35. Frare, E.; Polverino de Laureto, P.; Zurdo, J.; Dobson, C. M.; Fontana, A. A Highly Amyloidogenic Region of Hen Lysozyme. *J. Mol. Biol.* **2004,** *340*, 1153-1165.
36. Mishra, R.; Sorgjerd, K.; Nystrom, S.; Nordigarden, A.; Yu, Y. C.; Hammarstrom, P. Lysozyme Amyloidogenesis is Accelerated by Specific Nicking and Fragmentation but Decelerated by Intact Protein Binding and Conversion. *J. Mol. Biol.* **2007,** *366*, 1029-1044.
37. Shen, Y. R. Surface-Properties Probed by Second-Harmonic and Sum-Frequency Generation. *Nature* **1989,** *337*, 519-525.
38. Fu, L.; Ma, G.; Yan, E. C. Y. In Situ Misfolding of Human Islet Amyloid Polypeptide at Interfaces Probed by Vibrational Sum Frequency Generation. *J. Am. Chem. Soc.* **2010,** *132*, 5405-5412.
39. Stockle, R. M.; Suh, Y. D.; Deckert, V.; Zenobi, R. Nanoscale Chemical Analysis by Tip-Enhanced Raman Spectroscopy. *Chem Phys Lett* **2000,** *318*, 131-136.
40. Anderson, M. S. Locally Enhanced Raman Spectroscopy with an Atomic Force Microscope. *Appl. Phys. Lett.* **2000,** *76*, 3130-3132.
41. Hayazawa, N.; Inouye, Y.; Sekkat, Z.; Kawata, S. Metallized Tip Amplification of Near-Field Raman Scattering. *Opt. Commun.* **2000,** *183*, 333-336.
42. Pettinger, B.; Picardi, G.; Schuster, R.; Ertl, G. Surface Enhanced Raman Spectroscopy: Towards Single Molecular Spectroscopy. *Electrochemistry* **2000,** *68*, 942-949.
43. Sonntag, M. D.; Pozzi, E. A.; Jiang, N.; Hersam, M. C.; Van Duyne, R. P. Recent Advances in Tip-Enhanced Raman Spectroscopy. *J. Phys. Chem. Lett.* **2014,** *5*, 3125-3130.
44. Mauser, N.; Hartschuh, A. Tip-Enhanced Near-Field Optical Microscopy. *Chem. Soc. Rev.* **2014,** *43*, 1248-1262.
45. Ichimura, T.; Fujii, S.; Verma, P.; Yano, T.; Inouye, Y.; Kawata, S. Subnanometric Near-Field Raman Investigation in the Vicinity of a Metallic Nanostructure. *Phys. Rev. Lett.* **2009,** *102*, 186101.
46. Deckert-Gaudig, T.; Deckert, V. Nanoscale Structural Analysis using Tip-Enhanced Raman Spectroscopy. *Curr. Opin. Chem. Biol.* **2011,** *15*, 719-724.
47. Jiang, S.; Zhang, Y.; Zhang, R.; Hu, C. R.; Liao, M. H.; Luo, Y.; Yang, J. L.; Dong, Z. C.; Hou, J. G. Distinguishing Adjacent Molecules on a Surface using Plasmon-Enhanced Raman Scattering. *Nature Nanotech.* **2015,** *10*, 865-869.
48. Chen, C.; Hayazawa, N.; Kawata, S. A 1.7 nm Resolution Chemical Analysis of Carbon Nanotubes by Tip-Enhanced Raman Imaging in the Ambient. *Nat. Commun.* **2014,** *5*, 3312.
49. Kurouski, D.; Deckert-Gaudig, T.; Deckert, V.; Lednev, I. K. Structure and Composition of Insulin Fibril Surfaces Probed by TERS. *J. Am. Chem. Soc.* **2012,** *134*, 13323-13329.
50. Kurouski, D.; Deckert-Gaudig, T.; Deckert, V.; Lednev, Igor K. Surface Characterization of Insulin Protofilaments and Fibril Polymorphs Using Tip-Enhanced Raman Spectroscopy (TERS). *Biophys. J.* **2014,** *106*, 263-271.
51. VandenAkker, C. C.; Deckert-Gaudig, T.; Schleeger, M.; Velikov, K. P.; Deckert, V.; Bonn, M.; Koenderink, G. H. Nanoscale Heterogeneity of the Molecular Structure of

Individual hIAPP Amyloid Fibrils Revealed with Tip-Enhanced Raman Spectroscopy. *Small* **2015,** *11*, 4131-4139.
52. Socrates, G. *Infrared and Raman Characteristic Group Frequencies*. 3rd edition ed.; John Wiley & Sons: New York, 2004.
53. Stewart, S. F., P.M. Surface-Enhanced Raman Spectroscopy Adsorbed on an Electrochemically Prepared Silver Surface. *Spectrochim. Acta A Mol. Biomol. Spectrosc.* **1999,** *55*, 1641-1660.
54. Blum, C.; Schmid, T.; Opilik, L.; Metanis, N.; Weidmann, S.; Zenobi, R. Missing Amide I Mode in Gap-Mode Tip-Enhanced Raman Spectra of Proteins. *J. Phys. Chem. C* **2012,** *116*, 23061-23066.
55. Kurouski, D.; Postiglione, T.; Deckert-Gaudig, T.; Deckert, V.; Lednev, I. K. Amide I Vibrational Mode Suppression in Surface (SERS) and Tip (TERS) Enhanced Raman Spectra of Protein Specimens. *Analyst* **2013,** *138*, 1665-1673.

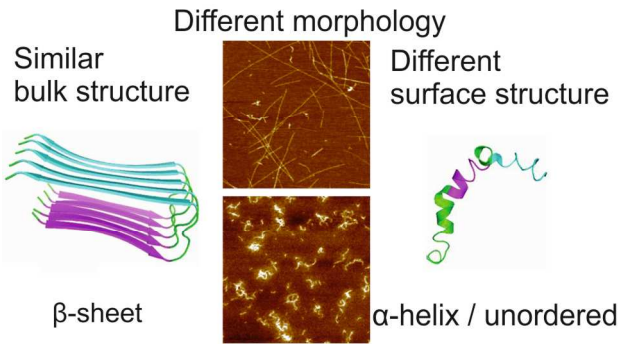
Different morphology
Similar
bulk structure
Different
surface structure
β-sheet
α-helix / unordered